PERGAMON

International Journal of Heat and Mass Transfer 43 (2000) 417–435

International Journal of HEAT and MASS TRANSFER

www.elsevier.com/locate/ijhmt

Heat transfer enhancement of finned oval tubes with staggered punched longitudinal vortex generators

Y. Chen, M. Fiebig, N.K. Mitra*

Institut für Thermo- und Fluiddynamik, Ruhr-Universität Bochum, D-44780, Bochum, Germany

Received 2 July 1998; received in revised form 6 April 1999

Abstract

Punched longitudinal vortex generators in form of winglets in staggered arrangements were employed to enhance heat transfers in high performance finned oval tube heat exchanger elements. Three-dimensional hydrodynamically and thermally developing laminar flow (Re = 300) and conjugate heat transfer in finned oval tubes were calculated by solving the Navier–Stokes and energy equations with a finite-volume method in curvilinear grids. Velocity field, pressure distribution, vortex formation, temperature fields, local heat transfer distributions and global results for finned oval tubes with two to four staggered winglets ($\beta = 30°$, $\Lambda = 2$, $h = H$) were presented and compared. Winglets in staggered arrangement bring larger heat transfer enhancement than in in-line arrangement since the longitudinal vortices from the former arrangement influence a larger area and intensify the fluid motion normal to the flow direction. For Re = 300 and Fi = 500, the ratios of heat transfer enhancement to flow loss penalty $(j/j_0)/(f/f_0)$ were 1.151 and 1.097 for a finned oval tube with two and four staggered winglets, respectively.

1. Introduction

Fins are applied to reduce the thermal resistance on the gas side of gas-liquid heat exchangers, e.g. a finned tube heat exchanger shown in Fig. 1(a). To improve the performance of heat exchangers, further heat transfer enhancement (HTE) of the fins is necessary. Mechanisms for passive HTE are: (1) developing boundary layers, (2) swirl and (3) flow destabilization. Wing-type longitudinal vortex generators (LVG) as sketched in Fig. 1(b) can generate all of them [1–4].

Three-dimensional flow structure between the fins around the tube is complex due to the formation of horse-shoe vortices near the front stagnation region of the tube, flow separation on the tube and recirculation in the tube wake with helical vortices [5–8]. The interaction of such flow structures together with the longitudinal vortices further complicates the flow field. There are various geometric parameters which affect the formation, development, shape and strength of the longitudinal vortices, [1,2]. The complicated flow structure and the numerous geometric parameters make the geometry optimization nearly impossible. Yet the large number of parameters offers the high potential for heat transfer enhancement as well as the high flexibility for the integration of longitudinal vortex generators into the primary heat transfer surfaces.

For finned circular tubes with a punched delta winglet pair (DWP) ($\beta = 45°$, $\Lambda = 1.5$, $h = H$) on the fin, experimental investigations on the streamwise and spanwise position of the DWP were made by Dong [9]. For a best performance of heat transfer enhancement

* Corresponding author. Tel.: +49-234-700-6444; fax: 49-234-709-4162.

E-mail address: mitra@vtp.ruhr-uni-bochum.de (N.K. Mitra)

0017-9310/00/$ - see front matter
PII: S0017-9310(99)00157-X

Nomenclature

a	thermal diffusivity, coefficient
A	area
B	width
h	convective heat transfer coefficient, height of the winglet
H	channel height
k	thermal conductivity
L	length
p	pressure
R_{Nu}	Nusselt number enhancement
R_p	thermohydraulic performance factor
t	time
T	Temperature
u, v, w	velocity components
x, y, z	Cartesian co-ordinates
α	central angle
β	angle of attack
Λ	aspect ratio of winglets
ξ, η, ζ	generalized co-ordinates
ϕ	general dependent variable
δ	fin thickness
ν	kinematic viscosity
ρ	density

Subscripts and superscripts

0	reference value
B	bulk
cs	cross section
f	fin
frt	frontal
ht	heat transfer
i, j, k	index
m	mean value
sp	span averaged
T	tube
*	dimensional (superscript)

Dimensionless parameters and variables

Bi	Biot number, $h^*\delta^*/k_\mathrm{f}^*$
f_app	friction factor, $\frac{\Delta p^*}{\rho^* u_0^{*2}/2}\,\frac{A_\mathrm{frt}^*}{A_\mathrm{ht}^*}$
Fi	fin parameter 1, $\frac{k_\mathrm{f}^*}{k^*}\,\frac{\delta^*}{H^*}$
Ft	fin parameter 2, $\frac{a_\mathrm{f}^*}{a^*}\,\frac{1}{Pe}$
j	Colburn j-factor, $\frac{Nu_\mathrm{m}}{RePr^{1/3}}$
$Nu_{z=\{0;1\}}$	Nusselt number, $\frac{\dot{q}_{z=\{0;1\}}}{(T_\mathrm{f}-T_\mathrm{B})}$
Pe	Peclet number, $Re\ Pr$
Rr	Prandtl number, ν^*/a^*
$\dot{q}$	fin heat flux, $\frac{\partial T}{\partial z}\|_{z=0} - \frac{\partial T}{\partial z}\|_{z=1}$
Re	Reynolds number, $\frac{u_0^* H^*}{\nu^*}$

with respect to pressure loss penalty, the DWP should be located immediately behind the tube with one tube diameter distance between the winglets. With this position, numerical investigations were performed by Sanchez [10], Bastani [11], Biswas et al. [12], and Fiebig et al. [7,8]. Bastini [11] and Biswas et al. [12] did not consider the conduction in fins, while Sanchez [10] and Fiebig et al. [7,8] simulated the conjugate heat transfer in the tube-fin configuration. The results of the numerical simulations show that DWP delays the flow separation from the tube, deflects the flow to the tube wake, drags the fluid from the recirculation zone (the 'dead water zone') to the main flow, intensifies with mixing by swirl, and thus enhances the heat transfer. For a finned flat tube with a mounted DWP, experimental investigations by Valencia [13] show that the effect of the DWP on heat transfer enhancement is more pronounced than for a finned circular tube, and the DWP should be located to the upstream side of the flat tube with a distance of two tube widths between the winglets. The above mentioned investigations applied one DWP for one tube-fin element.

In the earlier studies [14–20] characteristics of heat transfer enhancement and flow loss penalty in finned oval tubes with one to three in-line punched DWPs were investigated. The DWPs were punched out of the fins on both side of the tube. In the vicinity of the winglet, the local spanwise averaged Nusselt number enhancement is about 60% for a winglet upstream of the oval tube, and between 100 and 200% for a winglet downstream. But the swirling motion generated by the in-line winglets influence only about the half width of the flow passage. Further heat transfer enhancement should be possible by increasing the effective width of the longitudinal vortices. One way to do that is to increase the winglet length with constant angle of attack β and height h. This reduces the aspect ratio Λ of a winglet. The reduction of Λ below 1.5 lowers the thermohydraulic performance factor $(j/j_0)/(f/f_0)$ [14,16]. Another way to influence wider area by the vortex is to increase the number of longitudinal vortices in a cross section by increasing the number of winglets. To enhance the interaction of the longitudinal vortices, the winglets are staggered.

The existence of more than one longitudinal vortex would further complicate the flow structure and the

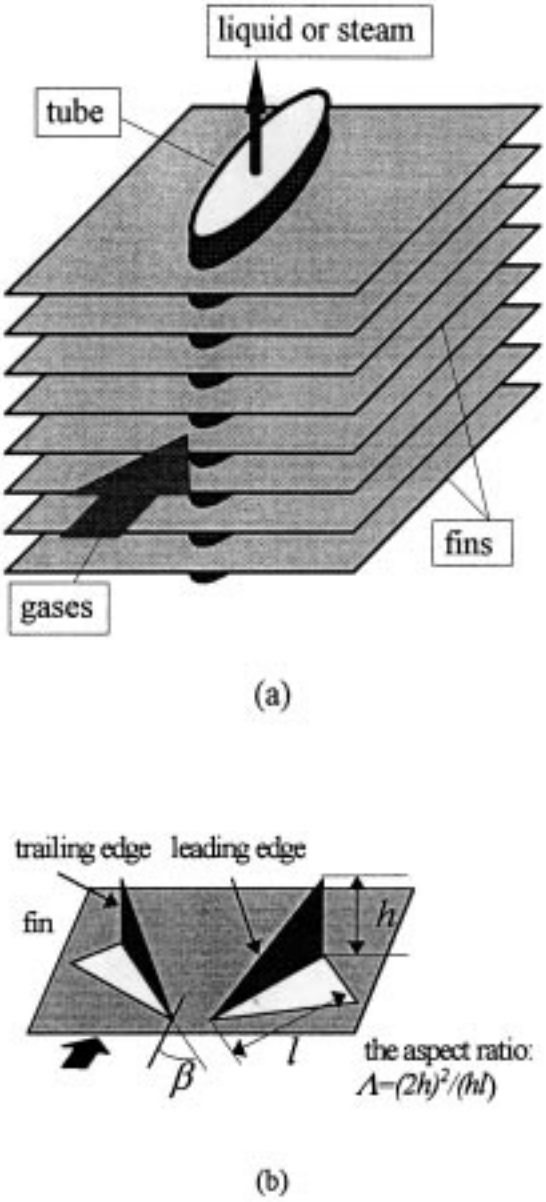

Fig. 1. (a) A finned oval tube heat exchanger element; (b) schematic of a delta winglet pair (DWP).

heat transfer behavior in the finned tubes. The interaction between the secondary flows generated by the tube and by the winglets, as well as the interactions of the longitudinal vortices by different winglets would play an important role on heat transfer enhancement and flow loss penalty. Such interactions have never been studied and provide the motivation of our work. The objectives of this paper are:

- to investigate the flow structure, temperature fields and heat transfer distributions in detail for finned oval tubes with two or four staggered winglets;
- to study the interaction of the secondary flows by investigating the flow patterns in detail;
- to study the effect of finite fin heat conduction on the fin heat transfer for Fi in the range of 100 and 1000;
- to compare the performance of finned oval tubes with in-line and staggered punched winglets.

2. Theoretical formulation and solution procedure

Fig. 2(a) shows a finned oval tube element with a DWP. Two fins with thickness δ form a channel of height H, width B ($=9.1H$) and L ($=15.4H$). An oval tube ($L_T/B_T=5.5$, cross sectional area $A_{T,CS}=24.6H^2$) is located at the center of the fin. The ratio of fin to tube area is 8.44. Such geometry is commonly used in industry [17]. Delta winglets are punched out of the fin to both sides of the tube. Two winglets as a pair are staggered by offsetting one of them a certain distance from the other in the streamwise direction. The thickness of the winglets is assumed to be zero and the height of the winglets (h) is equal to the channel height (H) so that the winglets can also function as pitch holders of the fins. The angle of attack β of the winglet is 30° and the aspect ratio Λ is 2, which are the results from an earlier investigation [14]. For small Reynolds numbers, the flow is steady and the computational domain can be reduced by using symmetry conditions on the mid-plane of the channel ($y=B/2$). Fig. 3(b) shows the computational domain and the boundary conditions employed. For a recirculation-free flow at the exit, the domain is extended by $6H$ from the exit of the element.

In this paper, flow patterns of five configurations (see Fig. 3(c)) were compared. There are two staggered winglets in configs. 12 and 13, three in-line winglets in config. 11, and four staggered winglets in configs. 14 and 15. The locations of the winglets are listed in Appendix A. The winglets near the tube are called winglets A, those away from the tube are called winglets B. For config. 14 and 15, the winglets upstream are called winglets A1 and B1, and those downstream are called winglets A2 and B2. In the geometrical model and computational domain in Fig. 2(a) and (b), only one DWP is shown. A finned oval tube without winglet is referred to as config. 0.

The velocity and temperature fields in the channel were calculated by solving the unsteady three-dimensional Navier–Stokes and energy equations for an incompressible fluid with constant properties by a time marching finite volume scheme. The temperature field in the fin was obtained by solving the conduction equation. The governing equations, the numerical

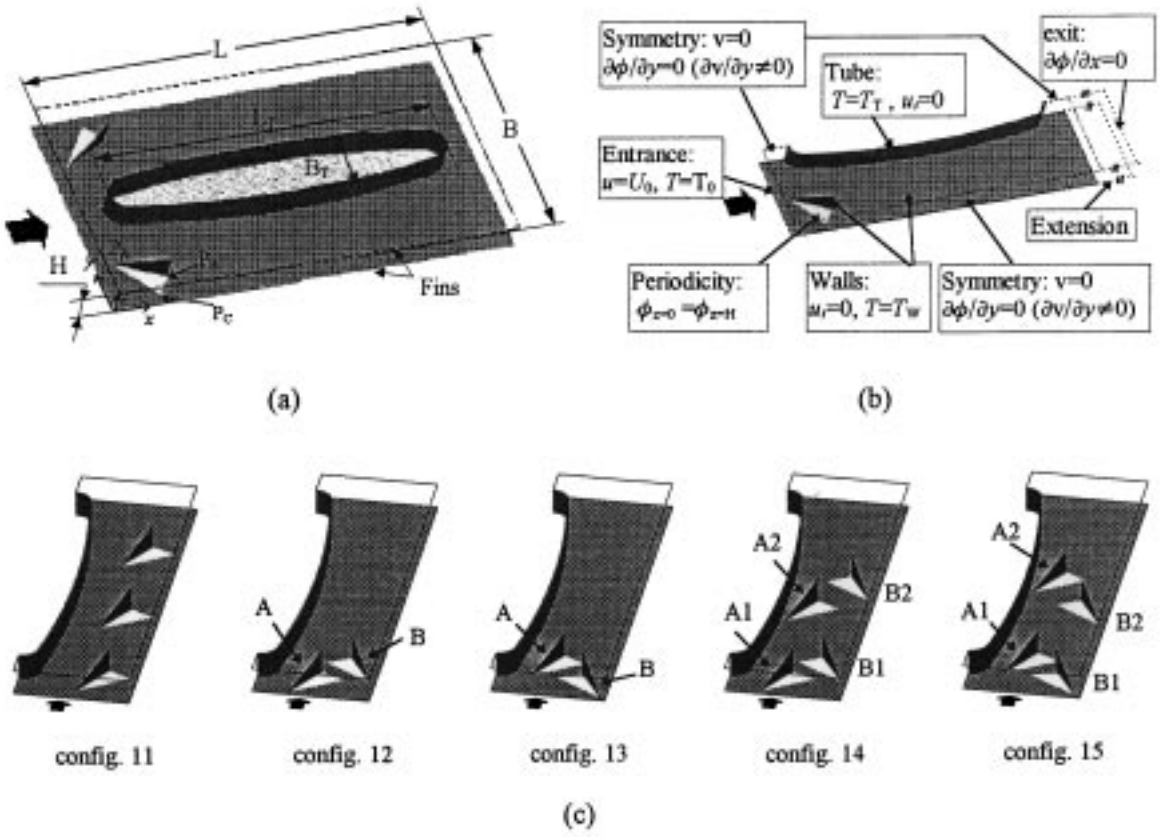

Fig. 2. (a) The geometrical model (L = 15.4, B = 9.1, $A_f/A_T = 8.44$, $L_T/B_T = 5.5$); (b) the computational domain with the employed boundary conditions; (c) the investigated configurations. In (a) and (b), only one DWP is shown. The area ratio of each winglet to fin is 1.73%.

method, the solution procedure, the grid points and the validation of the solution are identical to those presented in this journal [14,15,21] and will not be repeated here.

3. Results and discussions

3.1. Flow patterns

The results of the numerical simulations are the velocity, pressure and temperature fields. To demonstrate the flow structures, two types of streamlines are generated. The first type of streamline is two-dimensional for a certain cross section and was generated with the secondary flow (v, w), i.e. from the velocity components normal to the streamwise direction. This type of streamline illustrates the contour of the secondary flow, especially the longitudinal vortices, in a certain cross section. The second type of streamline is three-dimensional. Selected 3D streamlines clarify the structure of the longitudinal vortices.

Fig. 3(a) and (b) show vector-plots of the secondary flow and Fig. 3(c) and (d) the corresponding 2D streamlines in eight cross-sections of configs. 12 and 13 at Re = 300. In Fig. 3(a) and (b), the magnitude of the secondary flow generated by winglet B is larger, and the longitudinal vortices last longer than those by winglet A. The main reason for this is the larger local streamwise velocity due to the displacement by the tube. The secondary flow induced by the tube affected the longitudinal vortices of winglet A, so that until $x = L/2$, the magnitude of the secondary flow in the lower half of the longitudinal vortices is intensified, while in the upper half it is weakened (see Fig. 3(a) and (b)). For $x > L/2$, the opposite occurred. In the exit section, the 2D streamlines of the secondary flow by winglet A have even an opening near the bottom channel wall (see Fig. 3(c) and (d)), indicating the decay of the longitudinal vortices. The longitudinal vortices by winglet B were less affected by the second-

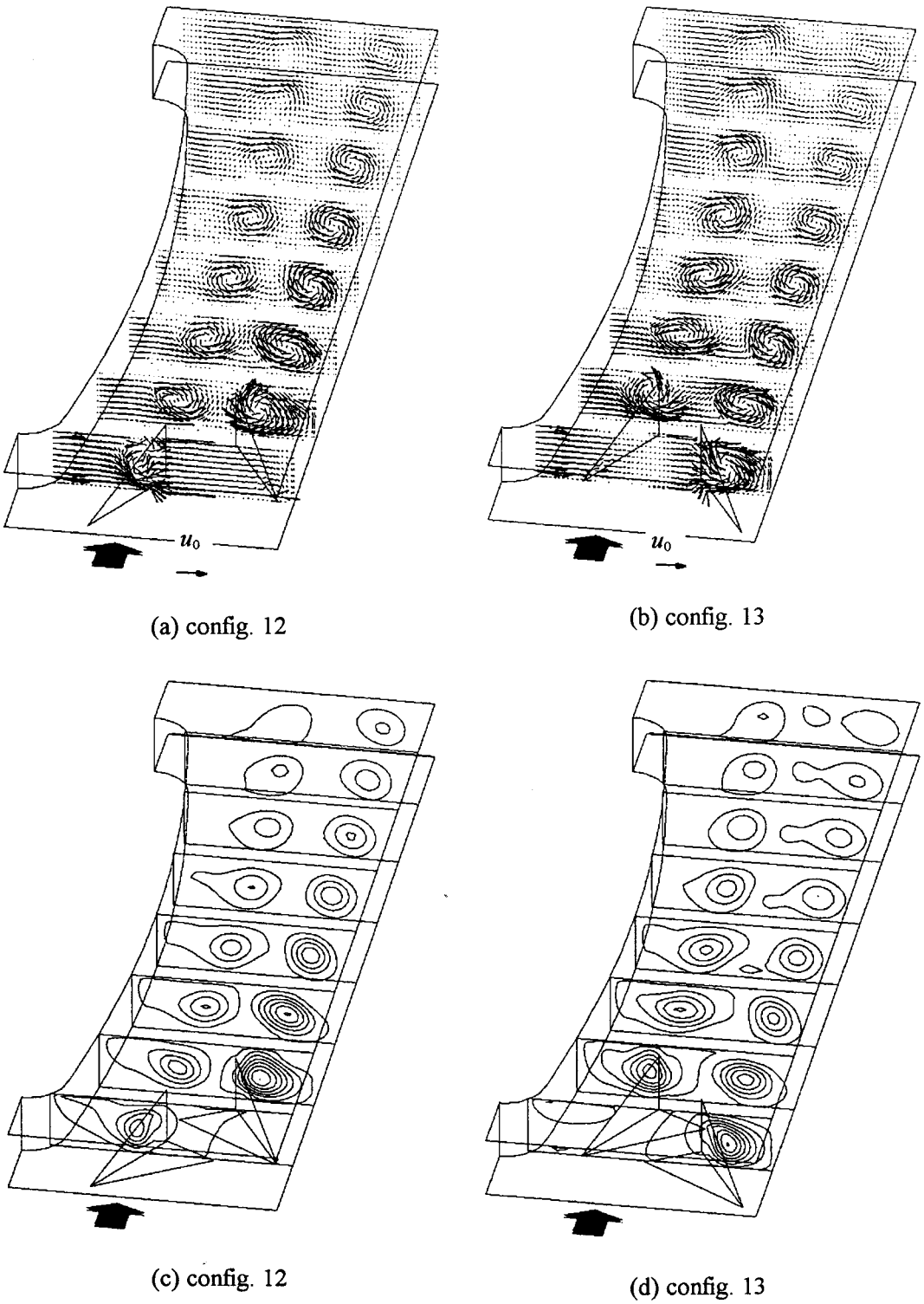

Fig. 3. Vector-plots of the secondary flow and the corresponding 2D streamlines on eight cross-sections in configs. 12 and 13 at $Re = 300$. The eight sections are located at $x = 1.5$, 3.5, 5.6, 7.7, 9.7, 11.8, 13.8, and 15.4, respectively.

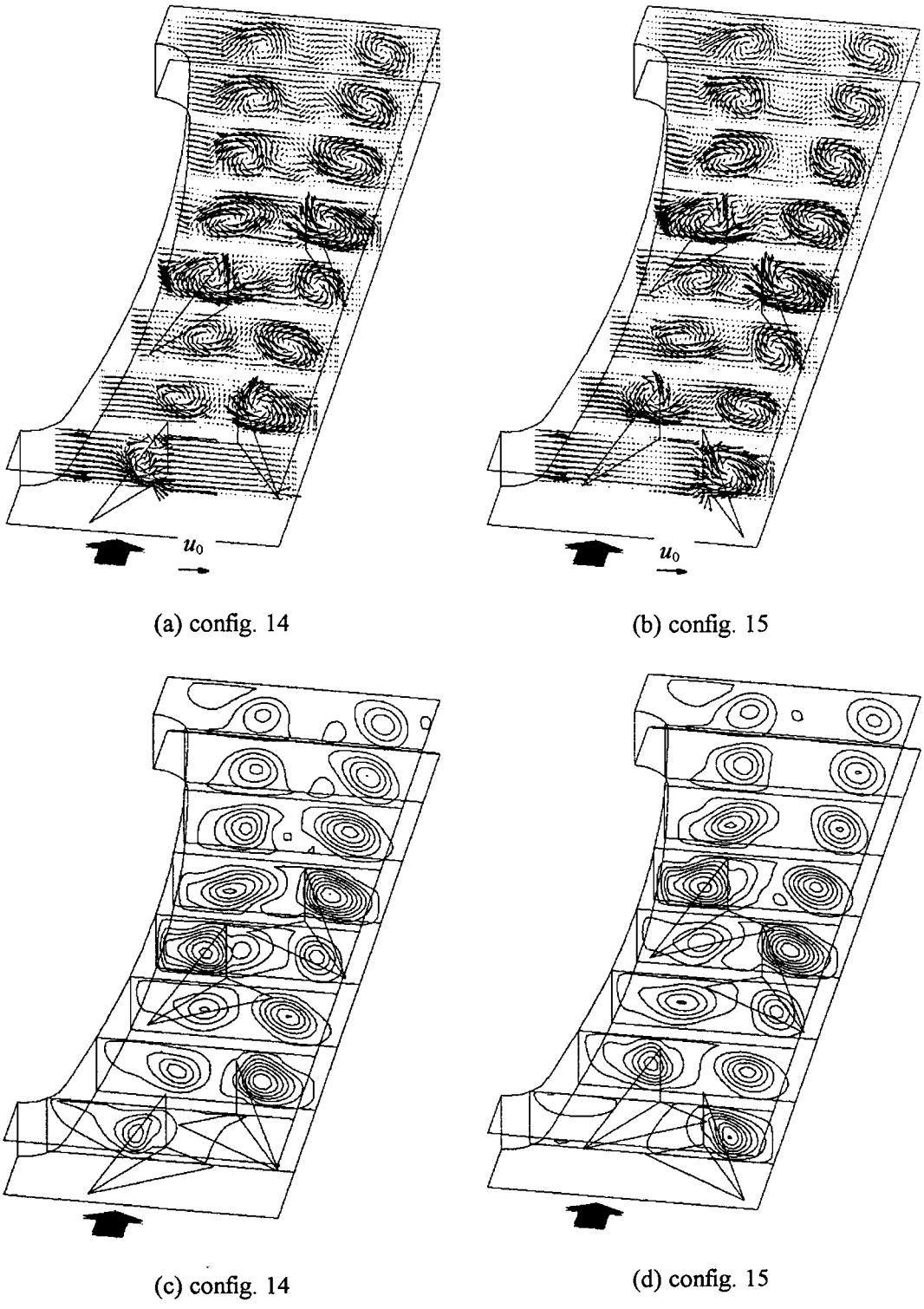

Fig. 4. Vector-plots of the secondary flow and their corresponding 2D streamlines in eight cross-sections in configs. 14 and 15 at $Re = 300$. The eight sections are located at $x = 1.5$, 3.5, 5.6, 7.7, 9.7, 11.8, 13.8, and 15.4, respectively.

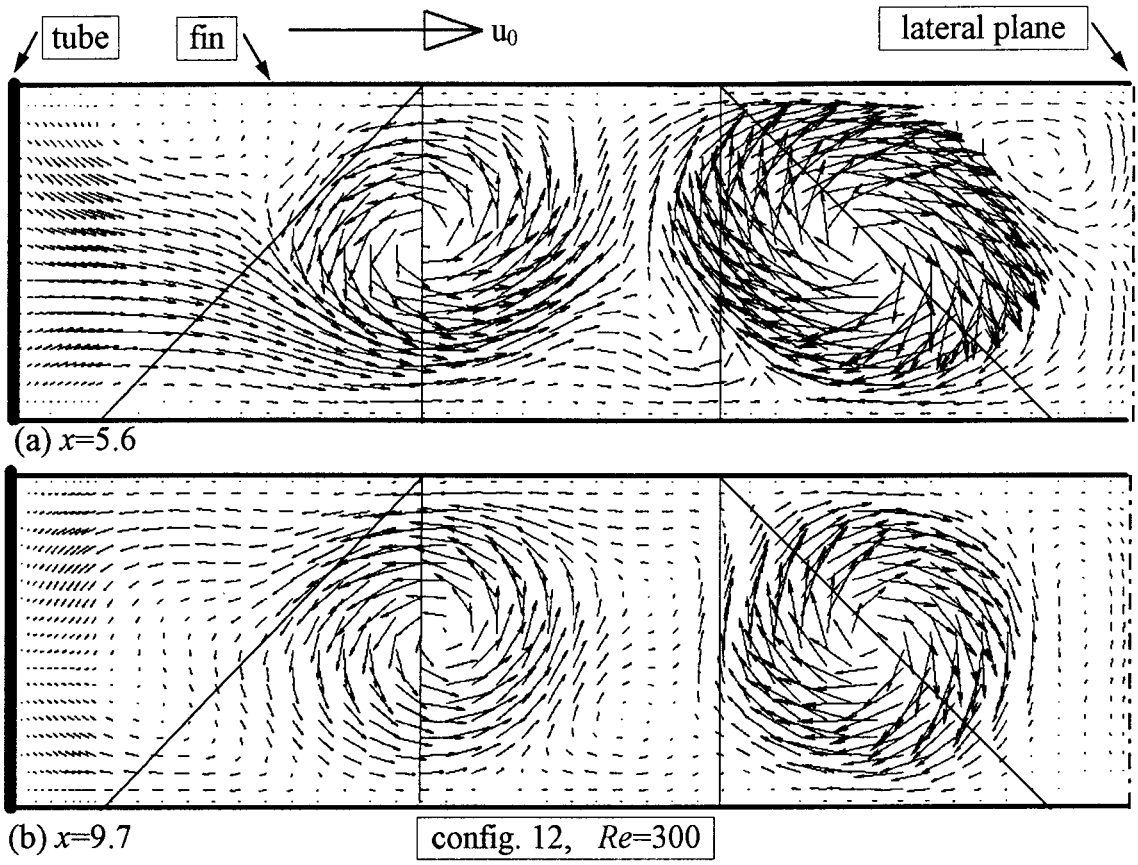

Fig. 5. Vector-plots of the secondary flow in two sections of config. 12 at Re = 300.

ary flow of the tube. In the fifth to eighth sections in Fig. 3(d), we see the formation of secondary longitudinal vortices between the primary longitudinal vortices. The flow became more complex if another two winglets were punched further downstream, as shown in the vector-plots of the secondary flow (Fig. 4(a) and (b)) and their corresponding 2D streamlines (Fig. 4(c) and (d)) in eight cross-sections of configs. 14 and 15 at Re = 300. Shortly behind winglet A2, two closely located vortical flow systems can be observed. The bigger one near the tube was generated by winglet A2 and the smaller one by winglet A1. The two co-rotating longitudinal vortices soon coalesce into one as also observed by Pauley and Eaton [22]. The longitudinal vortices generated by winglet B1 and B2 seem to coincide in a cross section because only one primary longitudinal vortices can be observed behind winglet B2. Downstream of winglet A2 and B2, strong interaction of the primary vortices, and secondary longitudinal vortices in the region between the primary longitudinal vortices, near the tube and near the lateral plane, can be observed, indicating further disturbance of the flow by winglets A2 and B2.

Fig. 5(a) and (b) are enlargement of the third and fifth sections in Fig. 3(a). The interaction of the flow around the tube and longitudinal vortices by the winglets can be observed. In Fig. 5(a), fluid near the tube is drawn to the lower part of the longitudinal vortices by winglet A, sent to the inter-region between the two primary vortices, and then partly circulated to the upper region of the same longitudinal vortex, partly driven to the upper region of the longitudinal vortices generated by winglet B and further swirled. This fluid motion intensifies the energy transport in the direction normal to the main flow. In Fig. 5(b), we see the complex flow structure in the region between the tube and the longitudinal vortex of winglet A as well as that between the two primary vortices.

In the cores of the longitudinal vortices, pressure minimum occurs as shown in Fig. 6 for the pressure distribution on the x–y-plane of z = 0.5 in configs. 12 and 15. Maximum pressures appear in front of the tube due to the stagnation and minimum pressures

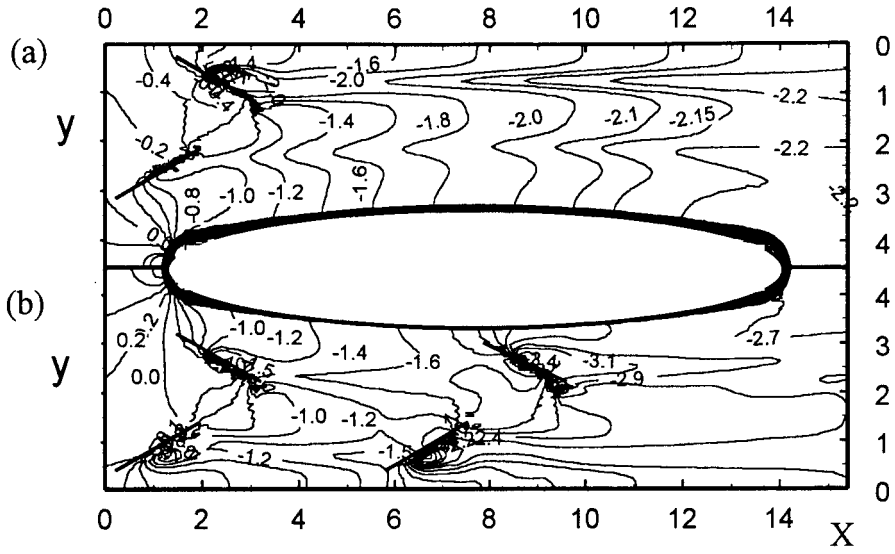

Fig. 6. Pressure distributions on the x–y-plane of $z = 0.5$ in (a) config. 12 and (b) config. 15 at $Re = 300$.

behind the winglet and in the tube wake. Compared to config. 15, the stagnation pressure in front of the tube of config. 12 is lowered by the winglet A. Pressure gradients from the vortex-core to its outer layer for winglets B are larger than those for winglets A, and those for the second winglet row are larger than those for the first row. For the longitudinal vortices by winglets A, the location of the pressure minimum in the y-direction changed slightly along the streamwise direction due to the displacement by the tube. For the longitudinal vortices generated by winglets B, no apparent change in the location of the vortex-core occurred. The space between the two primary vortices acts as a relaxation region for the two primary vortices, in which large pressure gradients appear.

Fig. 7(a)–(f) shows streamlines (SLs) on the vortex-cores and SLs from the leading edges of winglets in configs. 12 and 14. In Fig. 7(a) and (b), we see two longitudinal vortices swirling side by side down the stream. For winglet B, SLs on the vortex-core could be traced back to the front part of the leading edge, where flow separation begins, while for winglet A they scattered over the whole leading edge. The longitudinal vortices of winglet A and B differ from each other in the shape and manner of swirl, from the core to the outer regions, and from the formation to the development. These differences manifested themselves in the impact of the flow around the tube on the vortex flow of the winglets. Fig. 7(c) and (d) shows SLs on the vortex-cores by the winglets in config. 14. Their behavior was similar to those of config. 12. For winglets B1 and B2, the SLs could be traced back to the leading part of the leading edge, while for winglets A1 and A2, they scattered over the whole leading edge. The SLs on the vortex-core by winglet A1 passed winglet A2 around the trailing edge, while those of winglet B1 passed winglet B2 over the leading edge and joined the body of the longitudinal vortices by winglet B2. SLs of the vortex-core by winglet A2 stemmed from fluid in front of the tube, which was outside the longitudinal vortices by winglet A1, while those by winglet B2 stemmed from the fluid inside the longitudinal vortices by winglet B1. In Fig. 7(d), SLs on vortex-cores of winglets downstream were wrapped by those of winglets upstream, indicating that the vortex-cores by winglet B1 and B2 did not coincide in a cross section. This was not detected from either the vector plots or the 2D SLs of the secondary flow in Fig. 4. Fig. 7(e) and (f) shows the SLs from the leading edge of the winglets in config. 14. The longitudinal vortices by winglets B1 and B2 swirled faster than those by winglets A1 and A2. In Fig. 10(e), the longitudinal vortices from winglet B1 passed winglet B2 over the leading edge, partly accelerated and partly diverged. The longitudinal vortices from winglet A1 passed winglet A2 around the trailing edge. They were not accelerated, but diverged. From the combination of the SLs of the longitudinal vortex-cores by winglets A1 as well as B1 and the SLs from the leading edge of winglets A2 as well as B2 (Fig. 7(f)), we notice that the SLs in the wake of winglet B2 run more harmoniously than those in the wake of winglet A2.

3.2. Temperature fields and heat transfer

For oval tubes with plain fins (config. 0), the distri-

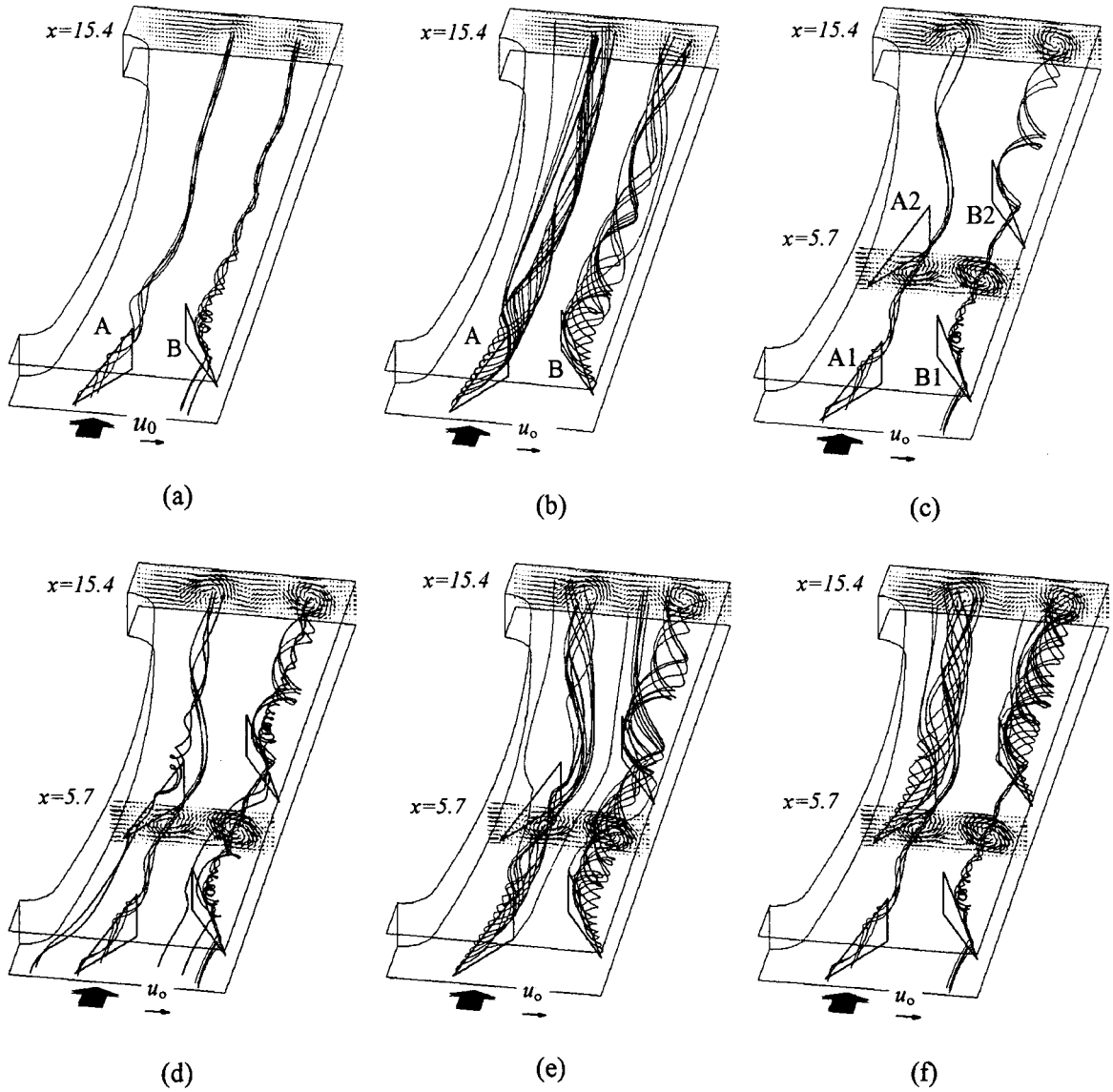

Fig. 7. (a) Streamlines on the vortex-cores and from the leading edges of the winglets in configs. 12 and 14 at $Re = 300$: (a) streamlines on the vortex-cores of the winglets in config. 12; (b) streamlines from the leading edges of the winglets in config. 12; (c) SLs on the vortex-cores of the winglets in the first row in config. 14; (d) combination of SLs on the vortex-cores of the winglets in the first and second row in config. 14 showing the interaction of the oncoming vortices and the new generated vortices; (e) SLs from the leading edges of the winglets in the first row in config. 14; (f) combination of SLs from the leading edges of the winglets in the second row and SLs in (c), showing the interaction of the oncoming vortices and the new generated vortices.

bution of fin temperatures are smooth [5,6]. With punched winglets, the fin temperatures on and around the winglets were lowered due to the enhanced heat transfer and the punched boundaries which break the heat conduction locally. Fig. 8 compares the fin temperatures in configs. 12–15 at $Re = 300$ and $Fi = 500$. For configs. 12 and 13, lower temperature regions near the leading edge of the fins appear, where winglets A and B were punched (Fig. 8(a) and (b)). For $x < 2$, the temperature near the lateral boundary in config. 13 is lower than that in config. 12. Fin temperatures were identical in the regions near the tube as well as in the tube wake and approximately the same in the rear part of fins for both configurations. For configs. 14 and 15 (Fig. 8(c) and (d)), two lower temperature regions appear, the one was caused by winglets A1 and B1

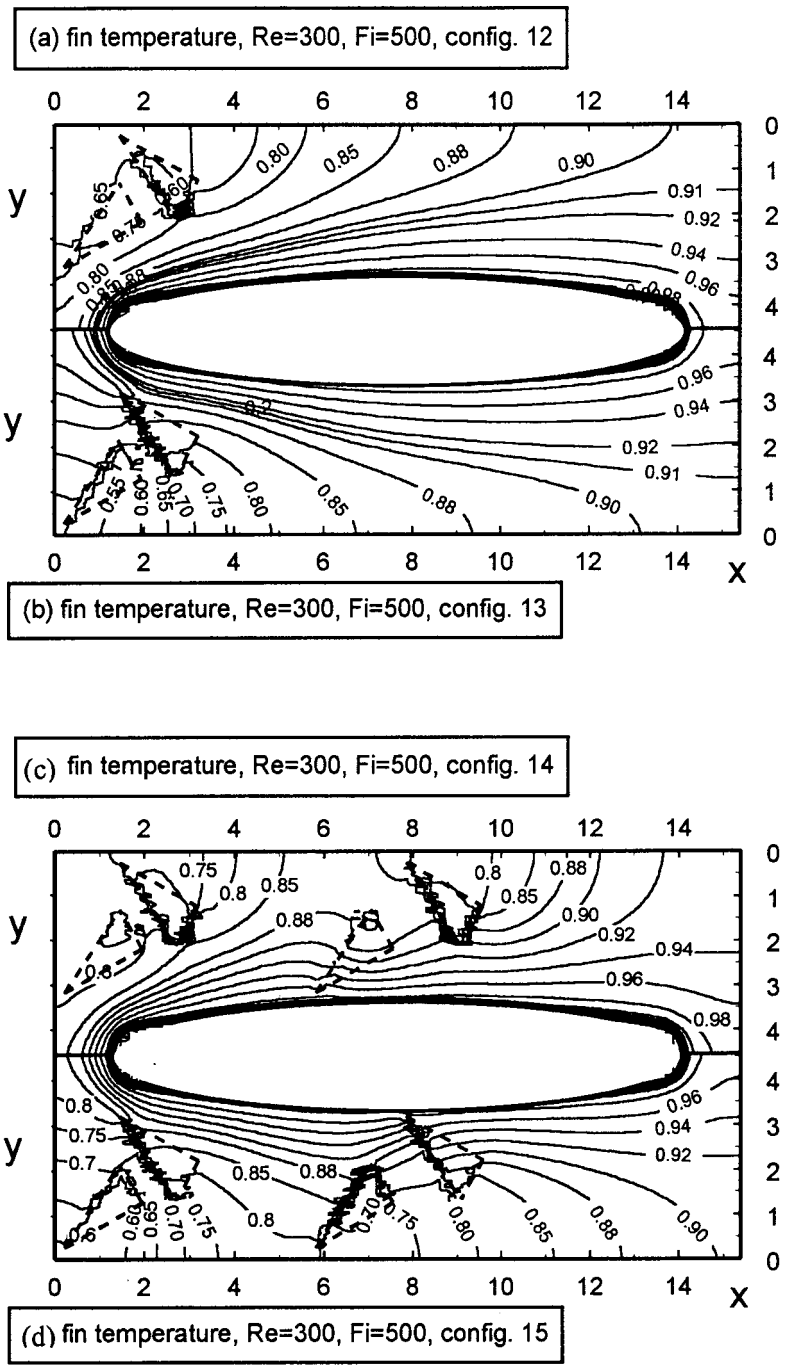

Fig. 8. Fin temperatures in configs. 12–15 and $Re = 300$ and $Fi = 500$. The dimensionless tube temperature $T_T = 1$.

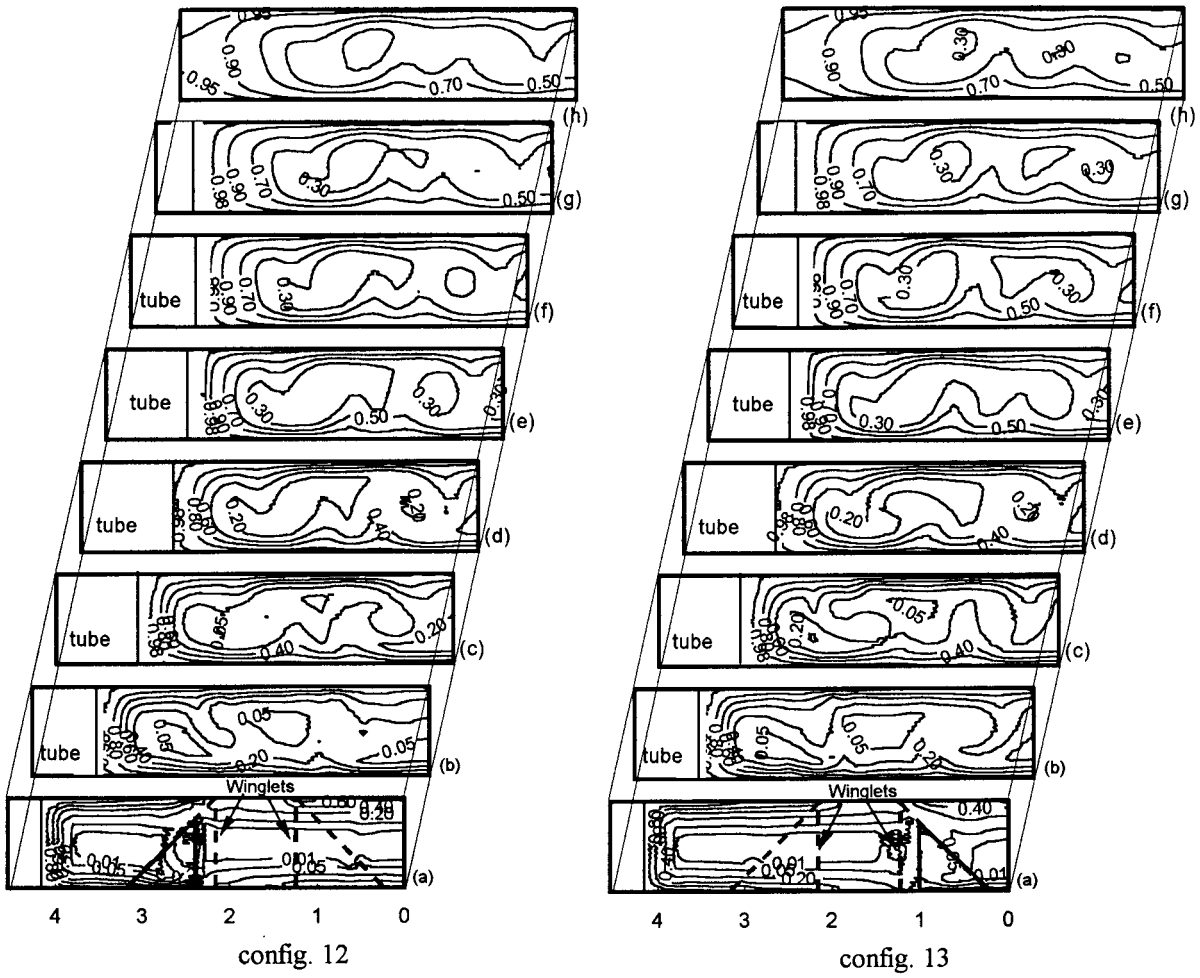

Fig. 9. Temperature distributions in eight sections of configs. 12 and 13 at $Re = 300$ and $Fi = 500$. The sections from (a) to (h) are located at $x = 1.5$, 3.5, 5.6, 7.7, 9.7, 11.8, 13.8, and 15.4, respectively. Temperature on the tube $T_T = 1$, at the entrance $T_0 = 0$. Solid or dashed lines indicate that (the parts of) winglets are located upstream or downstream of the respective sections.

near the leading edge of fins, and the other in the middle of fins by winglets A2 and B2. Comparing Fig. 8(a) with (c) and Fig. 8(b) with (d), we notice that winglets A2 and B2 affected the fin temperatures not only in their downstream, but also in their upstream to the proximity of winglets A1 and B1. Fin temperatures near the tube were also changed. Even the temperatures in the tube wake were not the same.

Fluid temperature isotherms in config. 0 show a U-shape [5,6]. This appearance was distorted by the swirling flow generated by the winglets. Fig. 9 shows the temperature distribution on eight sections of configs. 12 and 13 at $Re = 300$ and $Fi = 500$. A U-shape of the isotherms can still be traced in section (a) in spite of the restricted local disturbances. In the sections from (b) to (h), the U-shape was totally deformed. There are three thermal boundary layers, two on the fins, and one on the tube. Beginning with the section (b), the 'down-wash' and 'up-wash' effects on both sides of the longitudinal vortices and on both fins are indicated by the two thinner and two thicker thermal boundary layers on the fins. On the lower fin, the distance between the thicker area of boundary layers, or the 'common flow up' area between the two primary longitudinal vortices, varied in the streamwise direction. Reasons for this are the unequal formation and development of the longitudinal vortices generated by winglets A and B as well as the displacement effect of the tube. The divergence of the longitudinal vortices may also play a role. A pulling effect of the two vortical flow systems with 'common flow up' resulting from their image flows [22] may not be the case because the

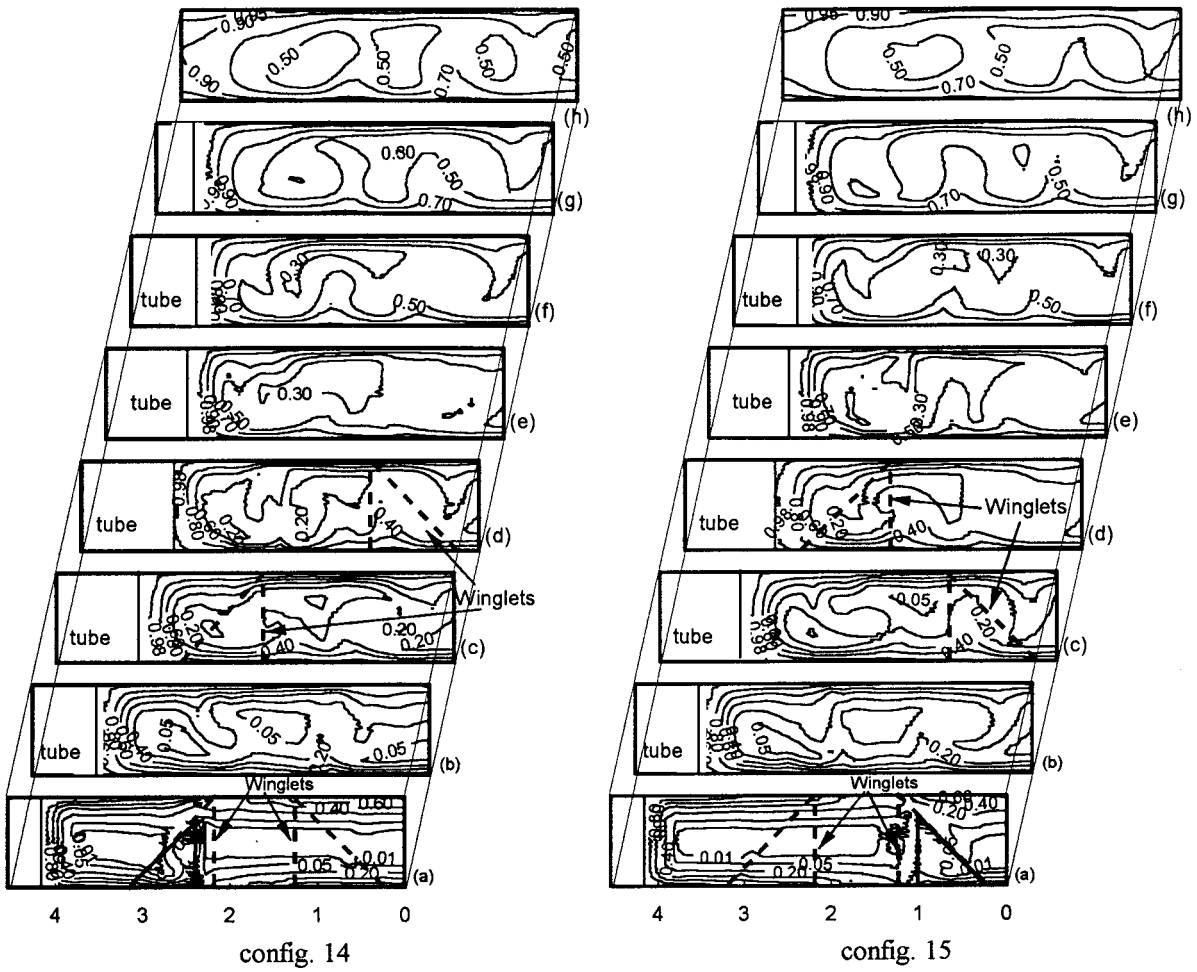

Fig. 10. Temperature distributions in eight sections of configs. 14 and 15 at $Re = 300$ and $Fi = 500$. The sections from (a) to (h) are located at $x = 1.5$, 3.5, 5.6, 7.7, 9.7, 11.8, 13.8, and 15.4, respectively. Temperature on the tube $T_T = 1$, at the entrance $T_0 = 0$. Solid or dashed lines indicate that (the parts of) winglets are located upstream or downstream of the respective sections.

winglet height was equal to the channel height and the longitudinal vortices ranged from the lower to the upper fins. So the image flows exist on both the lower and the upper fins with 'common flow up' and 'common flow down'. Despite the swirling flow, thick thermal boundary layers on the tube were observed indicating that heat transfers on the tube were not sufficiently enhanced. The distribution of the fluid temperatures in configs. 12 and 13 were different but the temperature levels were about the same. Fig. 10 shows the temperature distributions in eight sections of configs. 14 and 15 at $Re = 300$ and $Fi = 500$. A further distortion of the isotherms downstream of the winglets A2 and B2 can be observed. Beginning with section (d) in config. 14 and section (e) in config. 15, the boundary layers on the tube were thinned. Again the distribution of the fluid temperatures in configs. 14 and 15 were different but the temperature levels were about the same.

Fig. 11 shows the fin heat fluxes on the upper and lower channel wall for configs. 12 and 14 at $Re = 300$ and $Fi = 500$. The winglets are punched and connected to the lower channel wall. As mentioned above, thermal boundary layers were thinner in the 'down-wash' area and thicker in the 'up-wash' area, and correspondingly heat transfers were higher and lower in those areas. Because the longitudinal vortices cover the channel height, the 'down-wash' and 'up-wash' of the swirling flow occurs jointly on the upper and lower channel walls. On the upper channel walls (Fig. 11(a) and (c)), heat transfer in the area between winglets A and B was enhanced. On the lower channel walls (Fig.

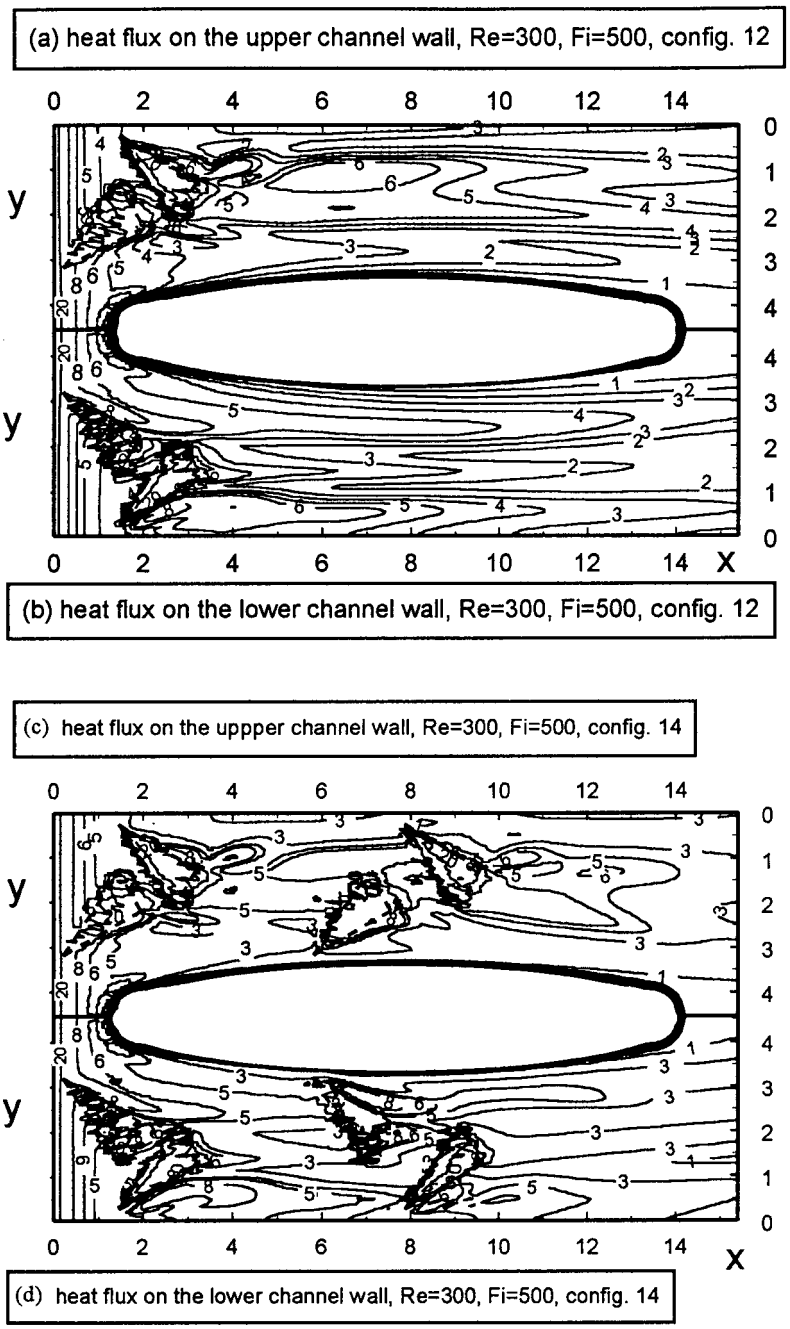

Fig. 11. Heat flux distributions on the upper and lower channel walls in configs. 12 and 14 at $Re = 300$ and $Fi = 500$.

11(b) and (d)), enhanced heat transfer appears in the area near the lateral boundary and near the tube, that are the areas behind the front part of the leading edges of the winglets. Heat transfers in the vicinity of the tube have not changed much in Fig. 11(a) and (b), but significantly enhanced in Fig. 4(c) and (d) by the longitudinal vortices generated by the winglet A2. The Nusselt number distribution on the fins shows the similar characteristics. The strong variation of heat fluxes on the surfaces of the winglets made it difficult to present them clearly in those areas.

For the investigated finned oval tubes without wing-

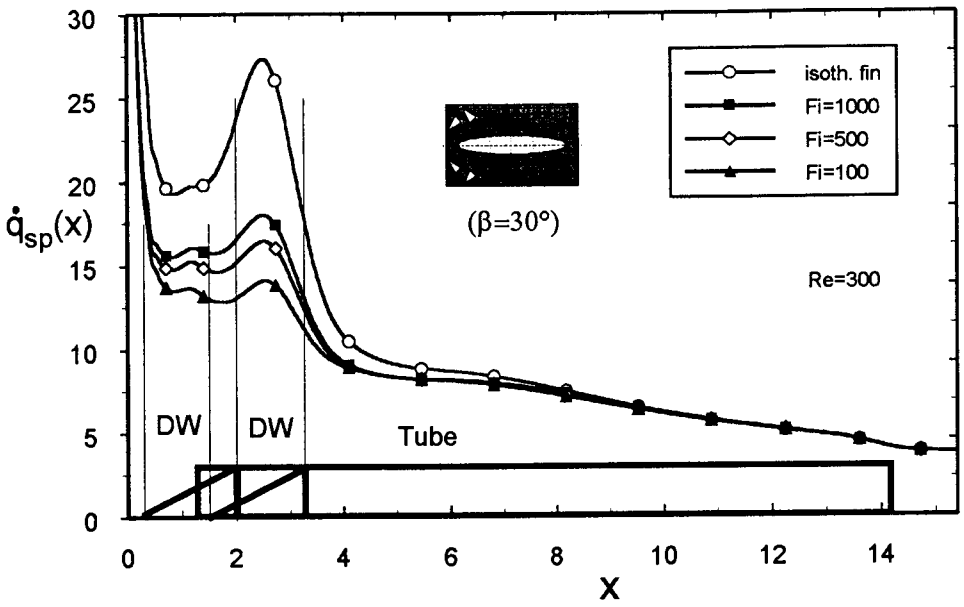

Fig. 12. Dependence of the fin heat fluxes on the fin parameter *Fi* in config. 12 at $Re = 300$.

let, the fin parameter *Fi* in the range of 100–1000 does not have a significant influence on the fin heat transfer [5,6]. For a finned oval tube with winglets, the effect of *Fi* was large because of the developing boundary layers on the winglets and the heat transfer enhancement by the swirling flow. Fig. 12 shows the dependence of the span-averaged heat fluxes $\dot{q}_{sp}(x)$ on *Fi* for config. 12 at $Re = 300$. The largest difference occurs in the proximity of the winglets, where heat transfer was largely enhanced and the fin temperature was lowered. In the position where local peaks occur, averaged heat flux $\dot{q}_{sp}(x)$ was reduced by 34.1, 39.9 and 48.4% for fins with $Fi = 1000$, 500, and 100, respectively with respect to the value of the isothermal fin. In the rear part of the fin, the difference is negligible.

Characteristics of heat transfer enhancement and flow loss penalty of finned oval tubes with in-line punched winglets were reported in [14,15]. The effective width of the longitudinal vortices was restricted for in-line winglets. Heat transfer enhancement was not so intensive even if three in-line winglets were employed for one tube-fin element. Fig. 13(a) compares the span-averaged Nusselt numbers enhancement $R_{Nu} = Nu/Nu_0$ with respect to config. 0 (Nu_0) in configs. 11 with three in-line winglets and in config. 12 with two staggered winglets at $Re = 300$ and $Fi = 500$. Similar tendencies of the Nusselt number enhancement appears for the first winglet in configs. 11 and 12. R_{Nu} by two closely located staggered winglets merges together, leading to a wider and higher peak in config. 12. For config. 11, R_{Nu} was stepwise increased by each winglet. In the range of x from about 8 to 10.5, heat transfer enhancements for configs. 11 and 12 were about the same, with that for config. 11 slightly higher. For a developing flow, generally a winglet located further downstream will exert higher local R_{Nu} than a winglet more upstream. For $x > 10.5$, R_{Nu} for config. 11 was enhanced once more and remained higher than that of config. 12. Global R_{Nu} was 1.40 and 1.50 for configs. 11 and 12 respectively. Fig. 13(b) compares the cross-sectional averaged pressure distribution in configs. 0, 11 and 12 at $Re = 300$. The additional pressure drop is mainly caused by the form drag of the winglet [23]. Comparing the curves, the form drag of the tube can be discerned. Immediately behind the winglets, a small increase in pressure can be observed, which resulted from a sudden expansion of the flow passage. The pressure level for config. 11 was stepwise lowered by three winglets. Up to $x \approx 1$, the three curves almost merge to one. Up to the trailing edge of the second winglet in config. 11, the curve for config. 12 is lower than that for config. 11. At $x = 4$, the additional pressure drop by config. 12 is 3.2 times that by config. 11, indicating a strong dependence of the form drag on the local streamwise velocity. In the range between the second and the third winglet in config. 11, the two curves for configs. 11 and 12 are almost combined to one. The pressure level for config. 11 was further lowered by the third winglet. Global dimensionless pressure drops over the elements were 1.70, 2.45 and 2.21 for configs. 0, 11, and 12, respectively at $Re = 300$.

Fig. 14 compares the spanwise averaged R_{Nu} in con-

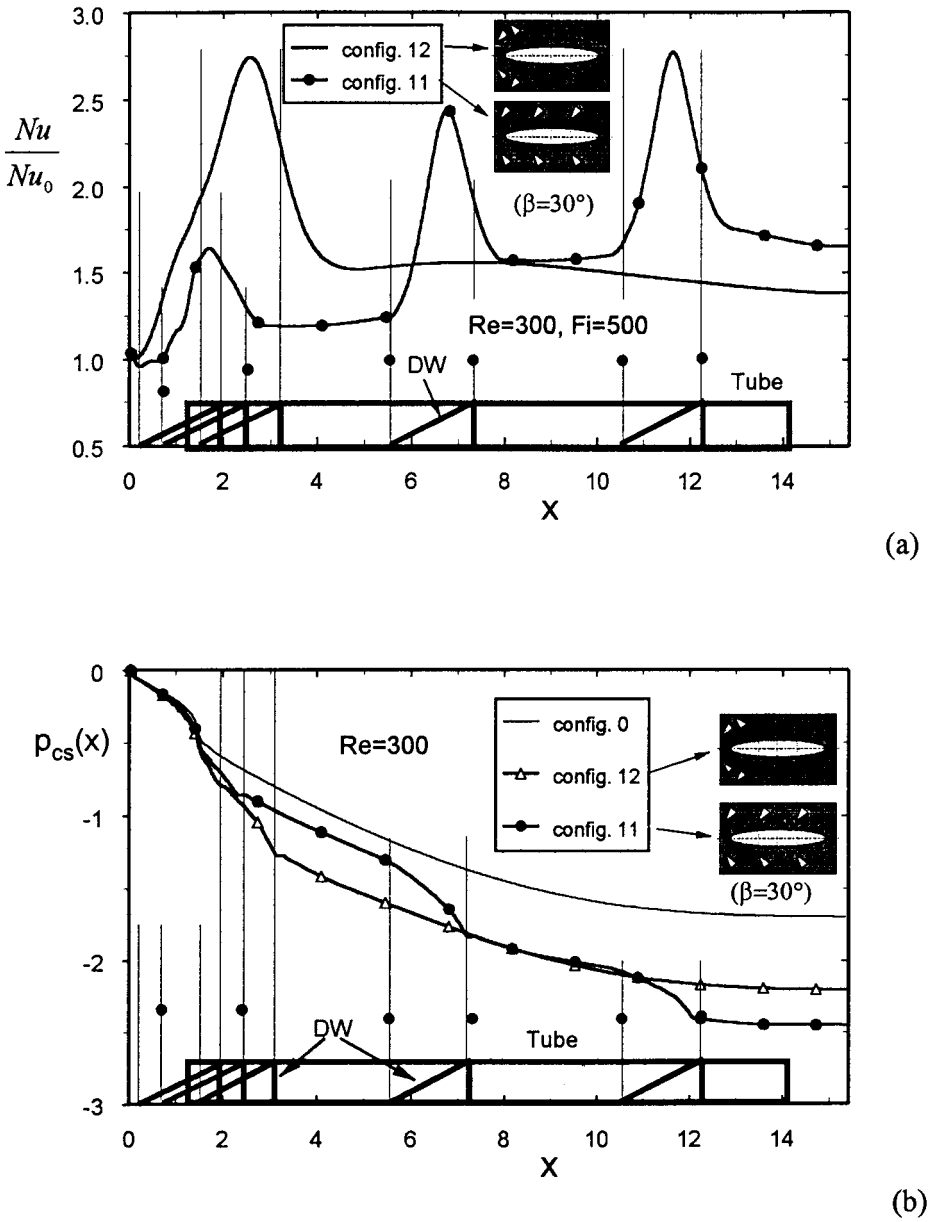

Fig. 13. Span averaged Nusselt number enhancements (a) and cross-sectional averaged pressure distributions (b) in configs. 11 and 12 at $Re = 300$ and $Fi = 500$.

figs. 12, 13, 14 and 15 at $Re = 300$ and $Fi = 500$. In Fig. 14(a), the peak for config. 12 is higher than that for config. 13. Downstream of $x \approx 4$, the difference is negligible. Global R_{Nu} was 1.50 and 1.49 for configs. 12 and 13, respectively. In Fig. 14(b), the peaks in downstream are higher than those in upstream for config. 14. Global Nusselt number enhancement for configs. 14 and 15 is surprisingly the same with $R_{Nu} = 1.87$. From the shape of the peaks in Fig. 14(a) and (b), it is clear that winglet B1 and B2 were more effective than winglet A1 and A2 in heat transfer enhancement. So for config. 15, the peak of the winglet B2 was higher than that of the winglet A2, though the winglet B2 was located upstream of the winglet A2. Reasons for that were: (1) the longitudinal vortices generated by winglets B1 and B2 are stronger than those by winglets A1 and A2, as demonstrated in the secondary flow vectors (see Figs. 3 and 4) and in the

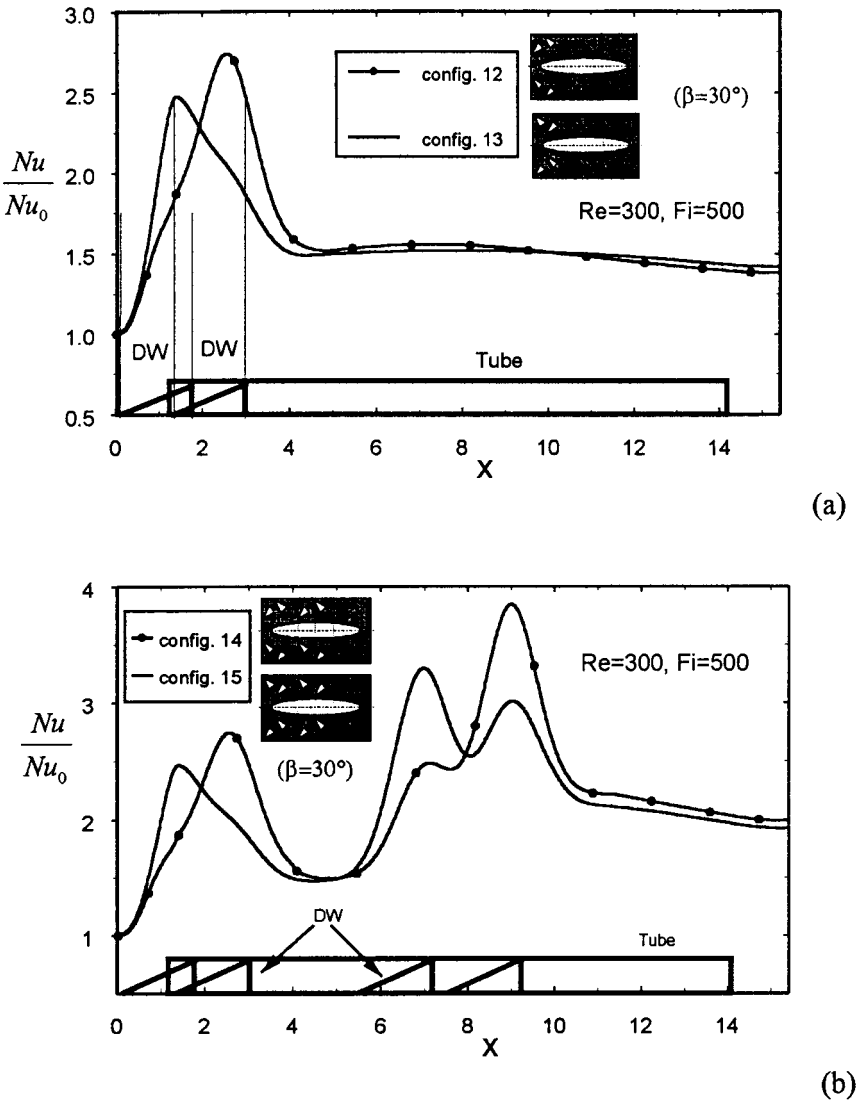

Fig. 14. Span averaged Nusselt number enhancements in configs. 12–15 at $Re = 300$ and $Fi = 500$.

streamlines of the swirling flow (see Fig. 7); (2) the longitudinal vortices generated by winglets B1 and B2 swirled the relatively colder fluid to the fin, while the longitudinal vortices generated by winglets A1 and A2 dragged the relatively warmer fluid near the tube (the heat source) to the fin (see Figs. 9 and 10).

Fig. 15 compares the spanwise averaged pressure distribution in configs. 12–15 for $Re = 300$. Downstream of the winglets, the difference of the pressure profiles for configs. 12 and 13 is negligible. At the exit, the pressure level for config. 12 is slightly lower than that of config. 13. Possible reason for this difference may be the changed flow structure near the tube. In Fig. 15(b), the pressure profiles for configs. 14 and 15 are very similar except for two local areas where small differences appear, one around $x \approx 2.5$ and the other around $x \approx 10$. At the exit, the pressure level for config. 15 is slightly lower than that of config. 14.

The thermohydraulic performance factor $R_P = (j/j_0)/(f/f_0)$ was equal to 1.151, 1.150, 1.097, and 1.086 for configs. 12, 13, 14 and 15, respectively at $Re = 300$ and $Fi = 500$.

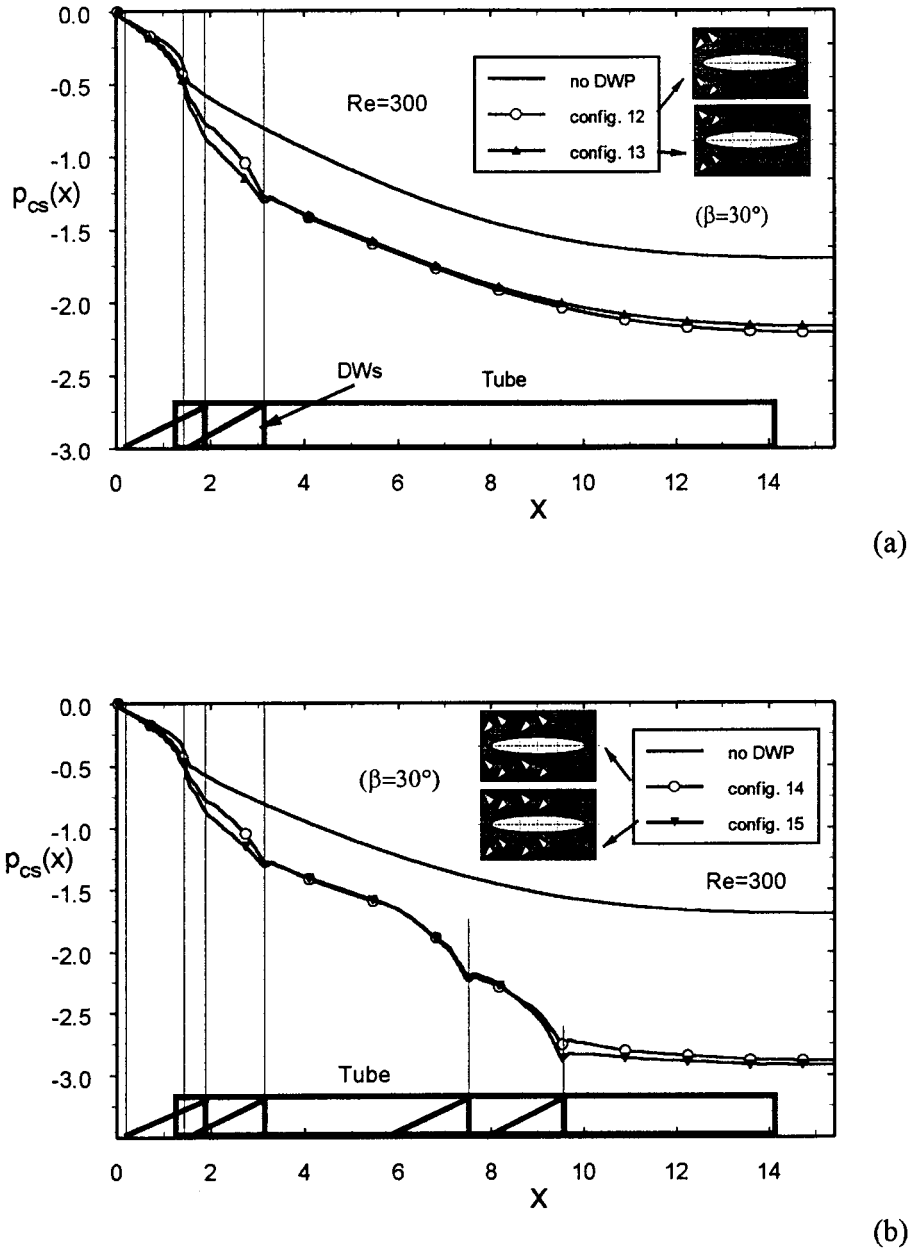

Fig. 15. Cross-section averaged pressure distributions in configs. 12–15 at $Re = 300$.

4. Concluding remarks

For the staggered winglets, the secondary flow induced by the tube and the no-slip boundary condition on the tube strongly affected the longitudinal vortices generated by the winglet near the tube. Longitudinal vortices generated by the winglet away from the tube were stronger and lasted longer. The interaction of the vortical flow generated by the staggered winglets intensified the fluid motion normal to the main flow direction.

- The staggered arrangement of the winglets was more effective than the in-line arrangement for heat transfer enhancement. Two staggered DWPs in config. 12 resulted in 20% higher heat transfer enhancement

with 14.5% lower additional pressure loss than three in-line DWPs in config. 11.
- With two and four staggered DWPs (configs. 12 and 14), Nusselt number was enhanced by 50% and 87% respectively with respect to plain fins at $Re = 300$ and $Fi = 500$.
- In a staggered arrangement, winglets B (the one away from the tube) were more effective than winglets A (the one near the tube) for heat transfer enhancement (Fig. 14);
- The temperature distribution in the flow passage was intensively distorted by the staggered longitudinal vortices (Figs. 9 and 10);
- *Fi* affected the heat transfer in the proximity of the winglets (Fig. 12).
- Slight relocation of the winglets hardly changed the performance of the winglets, as demonstrated by the performance comparison between configs. 12 and 13, or between configs. 14 and 15.

Appendix A

Locations of the winglets in the investigated configurations are shown below.

config.		x_{PA}	y_{PA}	x_{PB}	y_{PB}	x_{PC}	y_{PC}
11	1st winglet	0.63	2.19	2.36	1.19	1.86	0.32
	2nd winglet	5.55	2.19	7.28	1.19	6.78	0.32
	3rd winglet	10.47	2.19	12.2	1.19	11.7	0.32
12	Winglet A	0.2	3.185	1.93	2.185	1.43	1.319
	Winglet B	1.46	0.25	3.19	1.25	2.69	2.116
13	Winglet B	0.2	0.25	1.93	1.25	1.43	2.116
	Winglet A	1.46	3.185	3.19	2.185	2.69	1.319
14	Winglet A1	0.2	3.185	1.93	2.185	1.43	1.319
	Winglet B1	1.46	0.25	3.19	1.25	2.69	2.116
	Winglet A2	5.8	3.185	7.53	2.185	7.03	1.319
	Winglet B2	7.85	0.25	1.93	1.25	1.43	2.116
15	Winglet B1	0.2	0.25	9.58	1.25	9.08	2.116
	Winglet A1	1.46	3.185	3.19	2.185	2.69	1.319
	Winglet B2	5.8	0.25	7.53	1.25	7.03	2.116
	Winglet A2	7.85	3.185	9.58	2.185	9.08	1.319

References

[1] M. Fiebig, Vortex generators for compact heat exchangers, Int. J. of Enhanced Heat Transfer 2 (1995) 43–61.
[2] M. Fiebig, Embedded vortices in internal flow: heat transfer and pressure loss enhancement, Int. J. of Heat and Fluid Flow 16 (1995) 376–388.
[3] M. Fiebig, Vortices and heat transfer, Z. angew. Math. Mech. 77 (1997) 3–18.
[4] M. Fiebig, Vortices, generators and heat transfer, Trans. IChemE. 76 (Part A) (1998) 108–123.
[5] Y. Chen, M. Fiebig, N.K. Mitra, Conjugate heat transfer of a finned oval tube, part A: flow patterns, Numerical Heat Transfer, Part A 33 (1998) 371–385.
[6] Y. Chen, M. Fiebig, N.K. Mitra, Conjugate heat transfer of a finned oval tube, part B: heat transfer behavior, Numerical Heat Transfer, Part A 33 (1998) 387–401.
[7] M. Fiebig, A. Grosse-Gorgemann, Y. Chen, N.K. Mitra, Conjugate heat transfer of a finned tube, part A: heat transfer behavior and occurrence of heat transfer reversal, Numerical Heat Transfer, Part A 28 (1995) 133–146.
[8] M. Fiebig, Y. Chen, A. Grosse-Gorgemann, N.K. Mitra, Conjugate heat transfer of a finned tube, part B: heat transfer augmentation and avoidance of heat transfer reversal by LVG, Numerical Heat Transfer, Part A 28 (1995) 147–155.
[9] Y. Dong, Experimentelle Untersuchung der Wechselwirkung von Längswirbelerzeugern und Kreiszylindern in Kanalströmungen in Bezug auf Wärmeübergang und Strömungsverlust, Dissertation, Institut of Thermo- und Fluiddynamik, Ruhr-Universität Bochum, 1988.
[10] M. Sanchez, Numerische Simulation von einreihigen Lamellen-Rohr-Wärmeübertragern mit Längswirbelerzeugern, Dissertation, Institut für Thermo- und Fluiddynamik, Ruhr-Universität Bochum, 1991.
[11] A. Bastani, Numerische Untersuchung von Wärmeübergang und Strömungsverlust in Lamellen-

Rohr-Wärmeübertragern mit Längswirbelerzeugern, Dissertation, Institut für Thermo- und Fluiddynamik, Ruhr-Universität Bochum, 1992.

[12] G. Biswas, N.K. Mitra, M. Fiebig, Heat transfer enhancement in a fin-tube heat exchangers by winglet type vortex generators, Int. J. Heat Mass Transfer 37 (1994) 283–291.

[13] A. Valencia, Wärmeübergang und Druckverlust in Lamellen-Rohr-Wärmeübertragern mit Längswirbelerzeugern, Dissertation, Institut für Thermo- und Fluiddynamik, Ruhr-Universität Bochum, 1993.

[14] Y. Chen, M. Fiebig, N.K. Mitra, Conjugate heat transfer of a finned oval tube with a punched longitudinal vortex generator in form of a delta winglet—parametric investigations of the winglet, Int. J. Heat Mass Transfer 41 (1998) 3961–3978.

[15] Y. Chen, M. Fiebig, N.K. Mitra, Heat transfer enhancement of a finned oval tube with punched longitudinal vortex generator in-line, Int. J. Heat Mass Transfer 41 (1998) 4151–4166.

[16] S. Tiggelbeck, Experimentelle Untersuchungen an Kanalströmungen mit Einzel- und Doppelwirbelerzeuger-Reihen für den Einsatz in kompakten Wärmetauschern, Dissertation, Institut für Thermo- und Fluiddynamik, Ruhr-Universität Bochum, 1990.

[17] W.M. Kays, A.L. London, Compact Heat Exchangers, 3rd ed., McGraw-Hill Book Company, New York, 1984.

[18] Y. Chen, M. Fiebig, N.K. Mitra, Influence of the angle of attach of a wing-type VG on the heat transfer and flow loss of a finned oval tube, in: Proceedings of Eurotherm Seminar No 55, 'Heat Transfer in Single Phase Flows 5', Santorini, 18–19 September, 1997.

[19] Y. Chen, M. Fiebig, N.K. Mitra, Numerical investigation of fin efficiencies in a finned oval tube, in: Proceedings of the 15th IMACS World Congress, Wissenschaft und Technik Verlag, Berlin, 1997, pp. 761–766.

[20] Y. Chen, M. Fiebig, N.K. Mitra, Numerical investigation of flow and heat transfer in a finned oval tube, in: Proceedings of the Third ISHMT–ASME Heat and Mass Transfer Conference, Narosa Publishing House, New Delhi, London, 1997, pp. 735–740.

[21] R.K. Shah, M.S. Bhatti, Laminar convective heat transfer, in: S. Kakaç, R.K. Shah, W. Aung (Eds.), Handbook of Single-Phase Convective Heat Transfer, John Wiley & Sons, 1987.

[22] W.R. Pauley, J.K. Eaton, Experimental study of the development of longitudinal vortex pairs embedded in a turbulent boundary layer, AIAA Journal 26 (1988) 816–823.

[23] M. Fiebig, P. Kalweit, N.K. Mitra Wing type vortex generators for heat transfer enhancement. In: Proceedings of the Eighth IHTC, 1986, vol. 6, pp. 2909–2913.